Biocatalysis and Agricultural Biotechnology 19 (2019) 101129

Contents lists available at ScienceDirect

Biocatalysis and Agricultural Biotechnology

journal homepage: www.elsevier.com/locate/bab

Hydnocarpus alpina Wt extract mediated green synthesis of ZnO nanoparticle and screening of its anti-microbial, free radical scavenging, and photocatalytic activity

Mani Ganesh[a,b,**], Sung Gil Lee[b], Jayabalan Jayaprakash[c], Murugan Mohankumar[d], Hyun Tae Jang[a,*]

[a] Department of Chemical Engineering, Hanseo University, 360 Daegok-ri, Seosan-si, 356 706, Chungcheongnam-do, South Korea
[b] Department of Biological Sciences, Hanseo University, 360 Daegok-ri, Seosan-si, 356 706, Chungcheongnam-do, South Korea
[c] Department of Microbiology, St. Joseph's College of Arts and Science, Cuddalore, Tamil Nadu, India
[d] Micro Labs Limited, Bangalore, India

ARTICLE INFO

Keywords:
Hydnocarpus alpina (Wt)
ZnO NPs
Characterizations
anti-Microbial
DPPH scavenging
Photocatalytic activity

ABSTRACT

This paper reports green synthesis of ZnO nanoparticle (ZnO Np) using *Hydnocarpus alpina* aqueous alcoholic extract as capping agent. These green synthesized ZnO Nps were characterized using Fourier transform Infrared (FT-IR), powder X-ray diffraction (PXRD), Field Emission Scanning electron microscopy (FE-SEM), and UV–visible diffuse reflectance spectroscopy (DRS-UV). FE-SEM and PXRD results revealed that these synthesized ZnO NPs had spherical morphology with diameter of 38.84 nm and high phase purity. Gas chromatography–mass spectrophotometric (GC-MS) phytochemical fingerprinting analysis of the plant extract showed the presence of 19 phytoconstituents that might potentially act as stabilizing and capping templates in the formation of nano particles. These synthesized ZnO NPs were tested against various Gram (+) ve and Gram (−) ve microorganism. They were more active against *Proteus vulgaris* and *Salmonella enterica typhimurium* compared to other organisms studied. Furthermore, these ZnO NPs showed potential in scavenging 2,2-Diphenyl-1-picrylhydrazyl (DPPH) free radicals. They also possessed potential photocatalytic activity against methylene blue degradation of about 96% in basic pH. These results suggest that these green synthesized ZnO NPs using HA extract can be used as effective anti-microbial and photo catalysts for controlling pathogenic microbes and degradation of dyes in industrial effluents.

1. Introduction

Natural sources such as animal- and plant-derived medications have long been used to treat various human diseases and disorders in traditional medicine around the world. Of the reliable sources of natural products, plants and their secondary metabolites have long been viewed as one of the most precious sources. The plant kingdom provides a surplus of biologically active secondary metabolites; statistically, only about 10–15% of existing species of higher plants have been investigated for this purpose (Bisht et al., 2006). Among them, only about 6% have been screened for biological activity and medicinal utilization (Alcorn, 1995). In ancient times, people used plants as medicines based on their day-to-day experience and the trial and error method (Fakim, 2006). Approximately 80% of the world's population, particularly people in developing countries, still depend on herbal medicines for healthcare (Alcorn, 1995). Traditional healers of most medicinal systems followed in the world retain information about the medicinal value of plants in secret, and this information was usually only transferred to the next generation in secret. Hence, much information was lost or not retrievable. With the development of the field of ethnobotany, medicinal information on such plants was scientifically evaluated and transferred from traditional healers to the modern medicinal system by ethno-botanists (Alcorn, 1995).

Apart from the ethanobotanical view, plant extracts and their isolated secondary metabolites have recently been applied in various fields of research as an antioxidant, drug carrier, and as a reducer in metal and non-metal nanoparticle synthesis (Sharma et al., 2010; Ingale and Chaudhari, 2013; Sujitha and Kannan, 2013; Momeni et al., 2016).

* Corresponding author.
** Corresponding author. Department of Chemical Engineering, Hanseo University, 360 Daegok-ri, Seosan-si, 356 706, Chungcheongnam-do, South Korea.
E-mail addresses: chemgans@gmail.com (M. Ganesh), htjang@hanseo.ac.kr (H.T. Jang).

https://doi.org/10.1016/j.bcab.2019.101129
Received 28 December 2018; Received in revised form 21 March 2019; Accepted 9 April 2019
Available online 19 April 2019
1878-8181/

Synthesizing metal nanoparticles using a routine chemical procedure renders the process more hazardous and non-eco-friendly. However, the green synthetic route has rendered it more convenient and environmentally friendly through the utilization of plant extracts or microorganisms (biogenic) (Momeni et al., 2016; Fawcett et al., 2017). In this context, various metal and non-metal nanoparticles such as Silver (Ag NP), Gold (Au NP), Selenium (Se NP), Platinum (Pt NP), Zinc oxide (ZnO NP), and Copper Oxide (CuO NP) and bi metal nano particle such as ZnO/Ag and Ag/Au NPs have been synthesized in recent decades using various plants and their extracts and studied for the anti microbial, anti-biofilm and photocatalytic activity (Chen et al., 2008; Sharma et al., 2010; Ingale and Chaudhari, 2013; Sujitha and Kannan, 2013; Momeni et al., 2016; Anandalakshmi et al., 2016; Thaya et al., 2016; Fawcett et al., 2017; Saravanakumar et al., 2017; Anjugam et al., 2018a). Among the nanoparticles, ZnO NPs and functionalized ZnO NPs with have also been efficiently synthesized through green procedures and in an eco-friendly manner and studied for their anti-microbial properties, in the cosmetic field as UV filters, in catalysis as photo catalysts for the photo catalytic degradation of dyes and organics, and in the semiconductor field as light emitters (Chaudhuri and Malodia, 2017; Iswarya et al., 2017). Further the ZnO NPs and its functionalized forms were proved as micronutrient in increasing the immune responses and disease resistance in various fishes and cytotoxic to certain cancer cell (Anjugam et al., 2018a, 2018b). In considering the cost of raw material and the end product, ZnO NPs are more cost effective than Ag and Au NPs.

Hydnocarpus alpina Wt. (Flacourtiaceae) (HA), commonly known as 'Maravetti' in Tamil, is a large tree that grows up to 15–20 m tall and is found in the evergreen forests of India, Taiwan, and Southeast Asia (Parthasarathy, 1999). About 40 species belonging to the genus *Hydnocarpus* have been identified, among them *H. pentandra, H. macrocarpa, H. alpina, H. wightiana,* and *H. pendulus* are widely distributed in South India. The seed oil, commonly known as Hydnocarpus or chaulmoogra oil, is traditionally used in the treatment of leprosy (Kondal Reddy et al., 2013; Sahoo et al., 2014) as an alternative tonic, as well as in the treatment of cancer, rheumatism, sprains, braises, sciatica, and chest infections. Furthermore, the seed and its oil are used in the treatment of leucoderma, worm infection, polyuria, pruritus, eye diseases, sinus, and wounds. Recent reports have stated that *Hydnocarpus* possesses anti-inflammatory and hypoglycemic properties (Sahoo et al., 2014; Semwal et al., 2007; Jiangnan et al., 2013). Phytochemical analyses of hydnocarpus species have shown the presence of flavonoids, phenolics, tannins, coumarins, quinones, alkaloids, and steroids (Semwal et al., 2007; Jiangnan et al., 2013; Dhanasekaran et al., 2013). Balamurugan et al. isolated an active principle from the HA named 2R, 3R -Taxifolin 3-O-Rhamnoside, a flavonoid compound, and tested the hypoglycemic property of the isolated flavonoid using streptozotocin-induced diabetic rats, ultimately demonstrating its anti-diabetic activity (Balamurugan et al., 2014). The plant extract, as well its formulation in combination with neem oil, has potent anti-larvicidal and anti-feedant properties against *Spodoptera litura*, and has anti-microbial activities against various microorganisms (Dhanasekaran et al., 2013; Balamurugan et al., 2014; Ezhilvendan et al., 2010).

To the best of our knowledge, no study in the literature has focused on fingerprinting of phytoconstituents that are present in plant extracts by GCMS, the utilization of plant extract for green synthesis of ZnO nanoparticles, or anti-microbial activity of such nanoparticle. Hence, in the preset study, we performed fingerprinting analysis of aqueous alcoholic extract of aerial part of plant *Hydnocarpus alpina* using GC-MS and studied the usefulness of the extract for synthesizing ZnO nanoparticle and examined antimicrobial activity, 2,2-Diphenyl-1-picrylhydrazyl (DPPH) free radical scavenging activity, and photocatalytic activity for methylene blue (MB) degradation of such nanoparticle.

2. Materials and methods

2.1. Materials

Zinc nitrate hexa hydrate ($Zn(NO_3)_2$•$6H_2O$) was obtained from Daejung chemical and metals, Korea, 2,2-Diphenyl-1-picrylhydrazyl (DPPH) free radical was purchased from Sigma Aldrich, Korea, and all other chemicals used were procured from Dejung Chemical and metals, Korea, unless otherwise specified. In house-prepared double distilled DI water was used throughout the study.

2.2. Collection of plant and preparation of extract

Fresh aerial parts (leaf and stem bark) of HA plant were collected from Tirupati forest, Andhra Pradesh, India. A specimen of herbarium of HA was deposited at the Department of Botany of our university (voucher number 874). These collected plant materials were shade dried and powdered well. The powder was passed through Sieve (#40) to obtain a coarse powder suitable for extraction and then stored in airtight containers. Then 10 g of powder was taken to extract with ethanol water mixture (60:40) and ethanol (95%) separately. Ethanolic extract was used for GS-MS analysis.

2.3. Gas chromatography-mass spectrometry analysis

Gas chromatography-mass spectrometry (GC-MS) (Bruker Scion 436-GC) interfaced with a triple quadrupole mass spectrometer (TQ-MS) detector with a BR -5MS column (5% Diphenyl/95% Dimethyl poly siloxane, 30 × 0.25 mm × 0.25 μm df) was used for separation. For GC-MS detection, an electron ionization system with 70 eV ionizing energy, helium (99.999%) as the carrier gas at 1 mL/min constant flow rate, and an injection volume of 2 μLof sample was employed with a split ratio of 10:1; the injector and inlet temperatures were kept at 280 °C and 290 °C, respectively. The oven temperature was programmed from 110 °C (isothermal for 3.5 min) to 200 °C (no hold) at 10 °C/min increments, then 5 °C/min up to 280 °C and held for 12 min. Mass spectra of the extract were taken at 70 eV, with scan intervals of 0.5 s and fragments from 50 to 500 amu with the solvent delay of 0–3.5 min. The total GC run time was 40–50 min. The relative percentage amount of each component was calculated by comparing the average peak area to the total area. The software used for analyzing the mass spectra and chromatograms was MS work station.

2.4. Identification of compounds

The National Institute of Standards and Technology (NIST) data base (Version 11) with 62,000 patterns was used to compare the isolated peaks of the plant extract with known components spectrum in the library with reference to U.S. Department of Agriculture, Agricultural Research Service Dr Duke's, 1992–2016 (Dr Duke's,1992–2016).

2.5. Green synthesis of ZnO nanoparticles

After 0.016 mol zinc nitrate hexahydrate was dissolved in 50 mL of 10% aqueous ethanolic extract of HA, the solution was subjected to solvothermal reaction by keeping in an autoclave at 100 °C for 24 h. Then the autoclaved solution was then stirred under heating at 90 °C until a paste was obtained. The paste thus obtained was transferred to a silica crucible and heated at 100 °C in order to get a powder (as Synthesized ZnO). Finally the powder was subjected to calcination using a programmable muffle furnace at a ramp of 10 °C/min up to 500 °C. It was then kept isothermal for 4 h in order to remove the occluded organics. The obtained pale yellow powder (ZnO NPs) was then stored in an airtight container (Ramesh et al., 2015; Davar et al., 2015) until further use.

2.6. Characterization of ZnO nano particle

In order to investigate the formation of ZnO NPs, the as synthesized and calcined ZnO nano powder was subjected to Fourier-transform infrared spectroscopy (FTIR, Nicolet-200, Thermo Fishers Scientifics, USA) using the potassium bromide (KBr) pressed pellet technique. The shape, morphology, structure, and elemental composition of the synthesized ZnO NPs were assessed using Field Emission Scanning electron microscopy (FESEM, FEI Quanta200) coupled with energy dispersive spectroscopy (EDX). Morphological features and particle sizes of ZnO NPs were observed with a Hitachi tunneling electron microscope (Hitachi-800 TEM). NP dispersion was placed over a copper grid and allowed to dry. It was then placed in the TEM sample holder and analyzed. Diameters of these nanoparticles were measured using an image visualization software, Image J (National Institutes of Health, USA). Fibers loaded with AgNP's were also examined TEM. The powder X-ray diffraction (PXRD) pattern of the synthesized particle was screened using the Rigaku Miniflex diffractometer (Rigaku America, TX, USA) by scanning between 5° and 70° (2θ) with Cu Kα radiation (λ = 1.54 Å) in steps of 0.02° step. The diffuse reflectance UV (DRS Uv) spectra of the solid sample was recorded using Sinco Neosys 2000 UV (Korea) in DRS mode.

2.7. Antioxidant activities of synthesized ZnO NPs

The antioxidant activity of the ZnO NPs was accessed using the rapid Dot-blot procedure prescribed by Chang et al., with slight modification (Chang et al., 2007). As our ZnO NPs can only disperse in the diluting solvent, the method was slightly altered in the following manner: Standard Silica gel 6 F254 coated high performance thin layer chromatography (HPTLC, Sigma Aldrich, Korea) plates were cut to the desired dimensions and placed into a TLC developing chamber containing 0.1 mM 2,2-Diphenyl-1-picrylhydrazyl (DPPH) in 99% methanol, allowed to develop to a certain level, then dried naturally for 15 min at room temperature. Solutions of standard L-ascorbic acid, extract of the plant, and ZnO NPs at different concentrations (1, 0.5, and 0.25 mg/mL) were prepared in methanol. About 0.3 µL of each solution was then separately spotted over the plates and allowed to sit for several minutes, then the intensity of developed spots was manually observed (Chang et al., 2007; Shriniwas and Subhash, 2017; Jose and Radhamany, 2012).

2.8. Antibacterial studies

In order to evaluate the antibacterial potency of the synthesized ZnO NPs, agar-well diffusion method described previously (Saravanakumar et al., 2015; Iswarya et al., 2017) was used with slight modifications. Pathogenic microbial cultures used in this studies included Gram-positive (+) *Bacillus Subtilis (MTCC 441) and Micrococcus luteus (MTCC 106)* and Gram-negative (−) *Escherichia coli* (*MTCC 45*), *Proteus vulgaris* (*MTCC 1771*), *Shigella flexneri (1457), and Salmonella enterica typhimurium (1251)*. Muller Hinton agar was prepared and sterilized, then about 35 mL of the media was transferred to sterile petridish aseptically and allowed to solidify. After solidification, 100 µL of working stock cultures of the selected microbial strains (1.10^6 cells/mL) were spread with a sterile spreader, then left for several minutes without being disturbed. Wells were then made with a stainless steel borer. Differing volumes of the ZnO NPs suspension (1 mg/ml) equivalent to 10, 15, 20, and 25 µg of ZnO were then filled into the respective well of each microbial plate and kept in a refrigerator for 30 min in order to aid effective diffusion. The plates were then incubated at 37 °C for 24 h and the zone of inhibition on each plate was monitored.

2.9. Photo catalytic activity

Photo catalytic activity of prepared ZNO NPs carried out by following the procedure recommended by Habib et al. with little modification (Habib et al., 2012). To a 100 mL solution of the 20 mg/L methylene blue (Sigma Aldrich, Korea) dye, 100 mg prepared ZnO NPs was added and dispersed well by sonication and stirring. In order to monitor the reaction rate in various pH, the pH of the media was adjusted using acid (HCl and NaOH (0.1M)). The solutions of different pH were kept in a dark place so as to protect them from natural light induced degradation prior to exposure to light of 400 W tungsten lamp in the photo reactor. Blank solution without catalyst was also treated in the same way as solution containing catalyst. The solution was treated with a specific light source and the 3 mL samples were collected at specific time intervals, and degradation was monitored using a UV–vis spectroscopy instrument (Shimadzu UV-1700) at 665 nm. The samples collected were centrifuged at 4000 rpm for 10min before measuring the absorption spectra to remove the dispersed catalyst.

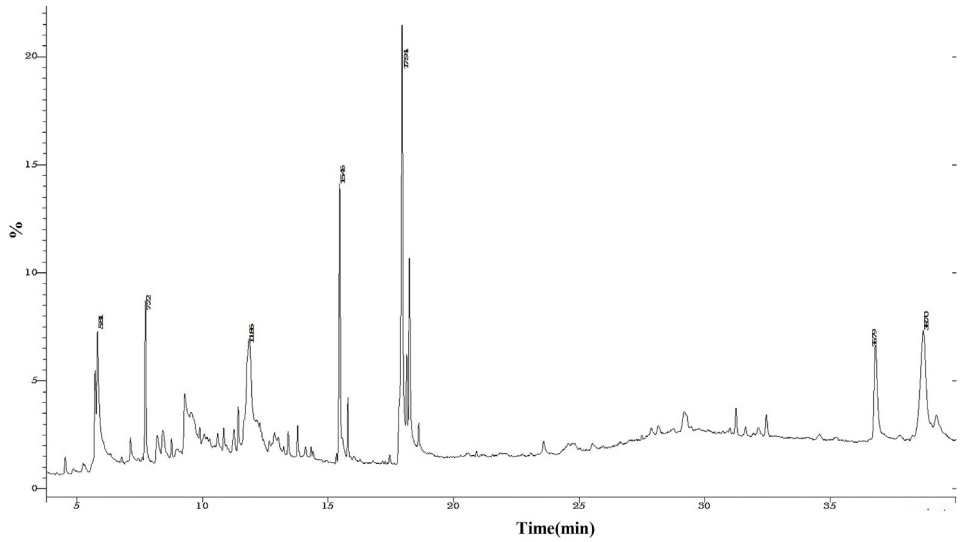

Fig. 1. GCMS –profile of HA extracts.

Table 1
List of compounds isolated and identified by GC-MS finger printing.

No	RT (min)	Name of the Compound	Mol.Formula	Mol.Wt	Peak Area (%)
1.	4.53	4H-Pyran-4-one,2,3-dihydro-3,5-dihyderoxy-6-methyl-	$C_6H_8O_4$	144	0.47
2.	5.72	Benzofuran,2,3-dihydro-	C_8H_8O	120	2.99
3.	5.81	5-Hydroxy methylfurfural	$C_6H_6O_3$	126	6.81
4.	7.13	5-isopropenyl-2-methylcyclopent-1-enecarboxaldehyde	$C_{10}H_{14}O$	150	0.68
5.	7.72	Eugenol	$C_{10}H_{12}O_2$	164	4.02
6.	8.41	1-[4-Hydroxymethyl-5-(2-mercaptomethyl)tetrahydrofuran-2-yl]-1-H-pyrimidine-2,4-dione	$C_{11}H_{16}N_2O_4S$	272	3.37
7.	9.29	3-Nitrophenyl)methanol,n-propyl ether	$C_{10}H_{13}NO_3$	195	4.33
8.	10.84	Syn-Tricyclo [5.1.0 (2,4)oct-5-ene,3,3,5,6,8,8-hexamethyl-	$C_{14}H_{22}$	190	2.65
9.	11.42	Megastigmatrienone	$C_{13}H_{18}O$	190	3.13
10.	11.86	n-Butyric acid 2-ethylhexyl ester	$C_{12}H_{24}O_2$	200	12.52
11.	15.46	n-Hexadecanoic acid	$C_{16}H_{32}O_2$	256	8.58
12.	15.79	Ethyl 13-methyl-tetradeconate	$C_{17}H_{34}O_2$	270	1.45
13.	17.94	9,12-Octadecdecadienoyl chloride, (Z,Z)-	$C_{18}H_{31}ClO$	298	17.19
14.	18.13	9,12Octadecadienoic acid, methyl ester	$C_{19}H_{34}O_2$	294	2.81
15.	18.24	Oleic acid	$C_{18}H_{34}O_2$	282	7.43
16.	18.61	Ethyl 14-methyl-hexadecnoate	$C_{19}H_{38}O_2$	298	1.20
17.	29.21	Cedran-diol, (8S,14)-	$C_{15}H_{26}O_2$	238	2.26
18.	36.79	β - Sitosterol	$C_{29}H_{50}O$	414	5.74
19.	38.70	Olean-12-en-28-oic,3-oxo-, methyl ester	$C_{31}H_{48}O_3$	468	12.37

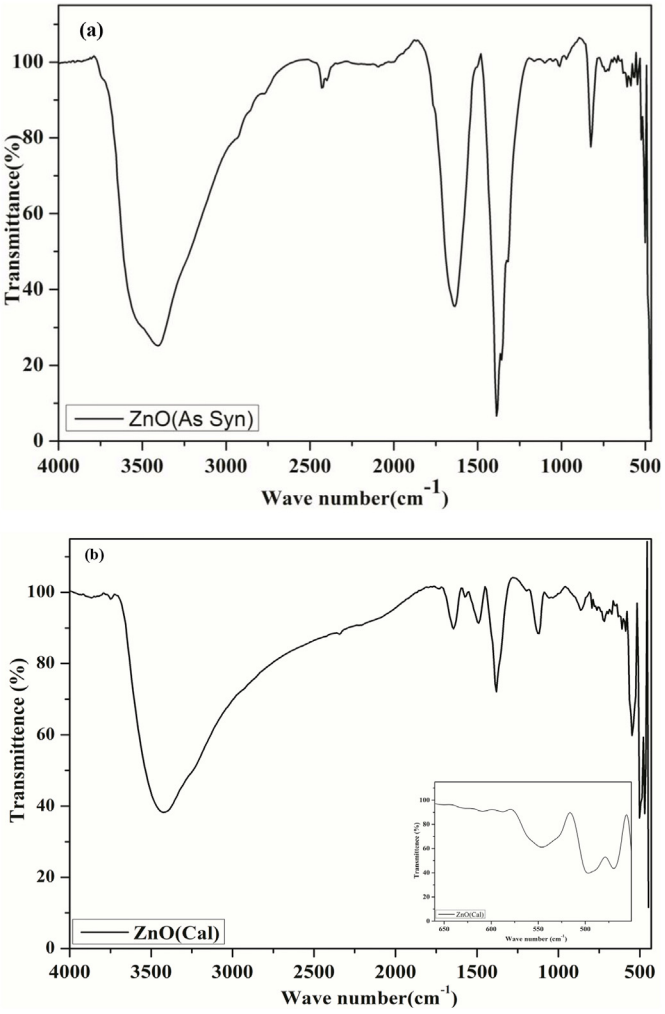

Fig. 2. FTIR spectra of (a) as synthesized ZnO NPs and (b) calcinned ZnO NPs.

3. Results and discussions

3.1. Gas chromatography-mass spectrometry (GC-MS)

A full scan gas chromatography-mass spectrometry (GC-MS) chromatogram of the ethanolic extract of the HA is shown in Fig. 1. The results show the presence of various bio active compounds in the extracts of HA. The plants were extracted using various solvent systems such as ethanol, methanol, and ethyl acetate. Ethanol was chosen for further study as the plant constituents were readily solubilized in it, and as it is cost-effective and non-hazardous. Based on the GC-MS analysis, about nineteen active principles were effectively separated. These active metabolites with respect to their retention time, molecular weight, and predicted molecular formulas are given in Table 1. Among them, 9,12-octadecdecadienoyl chloride, (Z,Z)- (17.19%), n-butyric acid 2-ethylhexyl ester (12.52%), olean-12-en-28-oic, 3-oxo-, methyl ester (12.37%), n-hexadecanoic acid (8.58%), oleic acid (7.43%), and 5-hydroxy methyl furfural (6.8%) were the major compounds with highest peak area percentages. Furthermore, the fragment 4H-Pyran-4-one, 2,3-dihydro-3,5-dihyderoxy-6-methyl isolated at the RT of 4.3 with a molecular weight of 144 resembles part of the structure of the 2R, 3R taxifolin 3-O-rhamnoside that was recently isolated and studied by Balamurugan et al., for its anti-diabetic activity (Balamurugan et al., 2014). Fig. S1 (in supplementary) represents the molecular structures of the major compounds that are separated with respect to the National Institute of Standards and Technology (NIST) database.

Table S1 (in Supplementary) shows the nature and biological activities of the isolated compounds, abridged from Dr. Duke's phytochemical and ethanobotanical database. The database shows that the compounds of 4H-pyran-4-one, 2,3-dihydro-3,5-dihyderoxy-6-methyl-(flavonoid fraction), benzofuran, 2,3-dihydro-(aromatic), 5-hydroxy methyl furfural (an aldehyde), and 5-isopropenyl-2-methylcyclopent-1-enecarboxaldehyde (phenolic) have antimicrobial, anti-inflammatory, and antioxidant properties. n-Butyric acid 2-ethylhexyl ester, n-Hexadecanoic acid, Ethyl 13-methyl-tetradeconate, 9,12-octadecdecadienoyl chloride, (Z,Z)-, oleic acid, and ethyl 14-methyl-hexadecnoate have potent anti-inflammatory, hypocholesterolemic, cancer preventive, hepatoprotective, nematicidal, insecticide, anti-histaminic, anti-eczemic, anti-acne, 5-Alpha reductase inhibitor anti-androgenic, anti-arthritic, anti-coronary, and insecticidal activity, while the major compounds such as 9,12-Octadecdecadienoyl chloride, (Z,Z)- a linoleic acid compound shows chemo preventive, hepatoprotective, anti-eczemic, and anti-acne activity. This demonstrates that this plant has the potential to extract many biologically active secondary metabolites.

3.2. Characterization ZnO NPs

3.2.1. FT-IR

Fig. 2 shows the FT-IR spectrum of the as synthesized ZnO NPs and

the calcined ZnO NPs. In the spectrum of as synthesized ZnO NPs, broad peaks are observed at around 3400 and 2350 cm^{-1}, representing the carbonyl and OH stretching caused by the presence of alcohol and phenolic acid, respectively. A shoulder peak near 3400 cm^{-1} assigned to NH may arise from the amino group and a peak at 1720 cm^{-1} may arise from the C═O group of esters and carboxylic acid. The peak near 1471 cm^{-1} was assigned to the CH bending vibrations of aldehyde or ketonic functionality. A peak at around 1150- 200 cm^{-1} is due to C—O—C vibration and the other peaks that are identified in the finger print regions (1110,1078, 975, and 789 cm^{-1}) are assigned to various aromatic functionalities that coexist in the extract. Similar vibrational bands were also observed in the FTIR spectrum of freeze-dried extract (Supplementary Fig. S2). From these results, it is evident that NPs are capped and stabilized with primary and secondary metabolites of the plant extract.

In the case of calcined ZnO NPs (Fig. 2(b)), a broad peak that was obtained near 3200 -3500 cm^{-1} was assigned to the OH stretching vibration of the physically adsorbed water or phenolic OH of polyphenol or flavonoids that remain after calcination. A peak due to carboxylic acid (COOH) tends to appear at around 1024 cm^{-1}, while peaks due to the asymmetric and symmetric stretching of Zinc carboxylate are observed at 1630 and 1384 cm^{-1}, respectively. This is due to the oxidation of reactive carbonaceous material during calcinations and the OH peaks are due to the surface adsorption of water over the surface of the calcined ZnO NPs. However, the peak intensity is weak when compared to as synthesized ZnO NPs. Transmittance to pure ZnO NPs appeared at around 460 and 505 cm^{-1}. The peak at 460 cm^{-1} represents the E_2 hexagonal mode of ZnO NP, which is shifted from its actual position of 435 cm^{-1}, potentially due to the organic remains from the extracts that are present over the ZnO NPs. The band at 509 cm^{-1} is due to the oxygen deficiency defects associated with ZnO (inset fig) (Xiong et al., 2006).

3.2.2. XRD

Fig. 3 depicts the powder X-ray diffraction (PXRD) patterns of the green synthesized ZnO NPs. The XRD spectra of the pale yellow colored green synthesized and calcined ZnO NPs were well matched with the ZnO wurtzite structure (JCPDS file No: 36–1451). XRD profiles of the synthesized sample reveal nine distinguishable Bragg's diffractions with the Miller indexation for the diffractions of (100), (002), (101), (102), (110), (103), (200), (110), and (201) at 2θ values of 31.29°, 33.95°, 36.04°, 47.03°, 57.01°, 62.28°, 66.91°, 67.45°, and 68.62°, respectively. The peaks were slightly shifted from their original positions but were comparable with the JCPDS file No: 36–1451 for hexagonal wurtzite crystallite structures (Xiong et al., 2006; Matinise et al., 2017). Further peaks representing other metals oxides were not observed in the obtained XRD, demonstrating that the sample produced here has high phase purity.

The crystallite average size Dp of the calcined ZnO NPs was calculated using Scherrer's formula $Dp = 0.9\lambda/\beta \cos\theta$, where λ is the wavelength of X rays used (1.54 Å), β is the full width at half maximum (FWHM), and θ is the angle of diffraction of the most intense peaks. The average particle size of the synthesized ZnO NPs was calculated to be 39.84 nm, which is in the order of nano size. Further, the high intensities observed in the XRD of the sample demonstrate that the ZnO NPs were highly crystalline. Based on the FT-IR and XRD results, the formation mechanism of the ZnO nano particle is postulated that the solvated Zn^{2+} ions that are ionized from the added zinc nitrate reacted with phytoconstituents such as phenolic and taxifolin-like flavonoids and give their corresponding organometallic chelating complex, which upon calcination will tend to become ZnO NPs. The properties and sizes of the synthesized ZnO NPs depend on the capping potential of the phytochemicals as well as the space they create between the Zn^{2+} (Matinise et al., 2017; Gawade et al., 2017). The reaction mechanism for the same was depicted in Supplementary Fig. S3.

3.2.3. DRS UV analysis

In order to determine the band gap of synthesized ZnO NPs, DRS UV was used, and the resulting DRS UV spectra of the sample are depicted in Fig. 4. In the spectra, an absorbance decrease is noted for the prepared ZnO NPs near 365 nm with an approximate inflexion at about 390 nm, which is equivalent of band gap value 3.2 eV (Matinise et al., 2017). This value is in good agreement with the band gap of pure ZnO crystals; the same inflection was not observed with commercial ZnO powder. This further demonstrates the phase purity of the synthesized sample, as explained previously in the section discussing the PXRD of the sample.

3.2.4. FE-SEM and TEM

Fig. 5(a–c) illustrate morphological characteristics of green synthesized calcined ZnO NPs. FE-SEM results showed that these nanoparticles were agglomerated to form a bigger particle with a layer-by-layer assembly which occurred during calcination. Microstructural analysis by FE-SEM at higher resolution showed that these ZnO NPs were clustered in a small spherical shape particle with smooth surface and particle size of 20–45 nm, similar to the particle size calculated from PXRD. To provide clear evidence of particle morphology, TEM was also carried out. Result is shown in Fig. 5(d). Results of TEM clearly showed that these particles synthesized were spherical in shape with an average size of 45 nm.

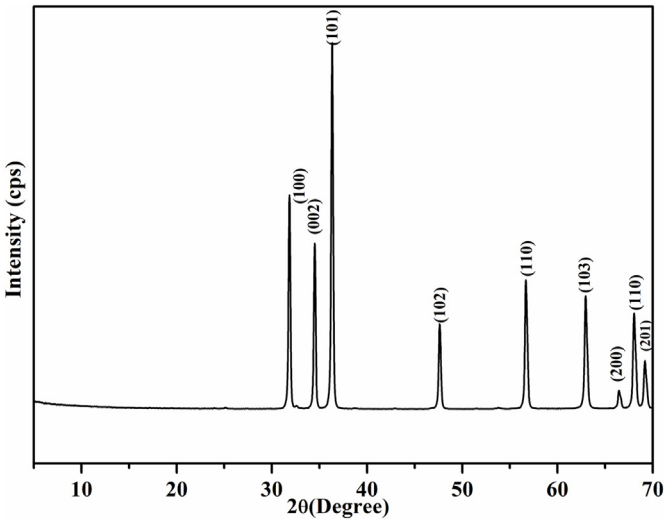

Fig. 3. PXRD traces of calcinned ZnO NPs.

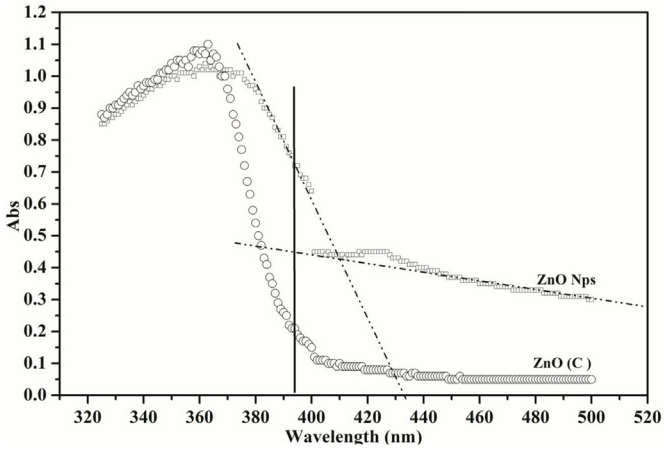

Fig. 4. DRS UV spectra of commercial ZnO (a) and (b) ZnO NPs.

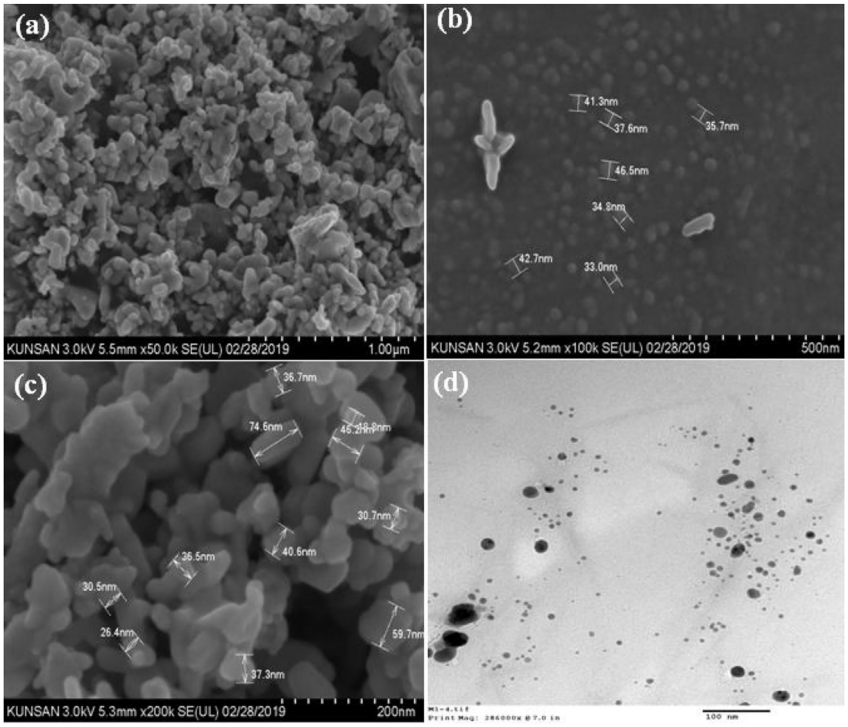

Fig. 5. FESEM(a) and TEM (b,c)images of ZnO NPs at various resolutions.

3.2.5. Energy dispersive X-ray (EDX) spectroscopy

Supplementary Fig. S4 shows the quantity of each element in the sample by EDX spectral analysis. Here, high values were found for the Zn and O, with 74.69% and 24.93%, respectively. A further peak is shown at around 2–3 eV, due to the gold element that was used for the sputtering, the omitted peaks near 0.5 eV are due to the carbon element doped over the particle, as previously explained in the sections discussing the FT-IR and XRD results. This higher value for zinc and oxygen shows that the synthesized ZnO NPs were phase pure compounds.

3.3. Antioxidant activity

The antioxidant efficacy of the ZnO NPs is given in Supplementary Fig. S5 this shows that the ZnO NPs have antioxidant potential to some extent. The intensity of the color of the spot developed varies from white to yellowish white in the case of the extract, which may be due to the color of the extract, as it is light yellow. However, in the case of ascorbic acid and ZnO NPs, the color is light yellow or white depending on the extent of antioxidant potential. Despite the lower color intensity of the ZnO NPs at the tested concentration, it is comparable with that of the extract and ascorbic acid at 3 µL of ZnO NPs (2 mg/mL).

3.4. Anti microbial activity

Fig. 6 shows the results of the antimicrobial activity of the synthesized nanoparticles. The inhibitory zones created by the particle show that their activity was concentration dependent, as the activity increased with increasing concentrations of the nanoparticle. The ZnO NPs synthesized using HA extracts are found to have the highest antimicrobial activity against *Proteus vulgaris* and *Salmonella enterica typhimurium* compared to the other microorganisms studied here. Compared to the gram (+)ve organism, the gram (−)ve organism shows clear and effective zones of inhibitions. Due to the thick protecting peptidoglycan layer covering the cell walls of gram (+)ve microbes inhibits or slows down the entry of the nanoparticle inside the cell wall (Reddy et al., 2014). In the case of gram (−)ve bacteria, the peptidoglycan layer is thin when compared to the gram (+)ve bacteria; hence, the nanoparticle can effectively enter the cell wall and chelates with the DNA entities of the microbes, thereby inhibiting their multiplication and growth. This does not occur in the bulk metal particle, as it requires an effective surface character and sufficiently small size to enable entry into the cell wall (Song et al., 2006; Emami-Karvani and Chehrazi, 2011).

3.5. Photocatalytic activity

The photo degradation of MB was studied by measuring the reduction in the intensity of absorbance of the dye at 665 nm in various time intervals from 10 to 30 min. The results showed that the intensity of absorbance produced by MB was reduced with increased time sof contact with ZnO NPs (Fig. 7). At the same time, there was negligible amount of reduction was noted in the absence of Zno NP (results not shown). In order to calculate the percentage degradation caused by the MB, the following equation is used:

$$\text{Percentage degradation} = \left(\frac{A_0 - A_t}{A_0}\right)100 \quad (1)$$

Where A_0 is the absorbance of the dye at time t = 0 and A_t is the absorbance of the dye at 10 and 30 min. The degradation observed in the absence of ZnO NPs is only about 7.6% even after 1 h. The results were comparable to previous reports (Mandal et al., 2018). In order to access the parameter that affects the catalytic activity such as temperature of calcination and pH of the media we compared the degradation caused by the ZnO NP synthesized by calcining at 400 and 500 °C along with commercial ZnO powder (Sigma, Korea), and changing the pH of the media using acid and bases. The results of the study showed that the sample calcined at 500 °C induced about 96.8%, whereas the sample synthesized at 400 °C and commercial ZnO showed slightly lower activity compared to the sample synthesized at 500 °C. This showed that the high temperature calcination caused a complete removal of organic templates from the extracts that produce finer particles with higher areas for contact with the dye when compared to others. In case of pH, the degradation at acidic pH of 4.8 was very low of about 5.8 at 30min,

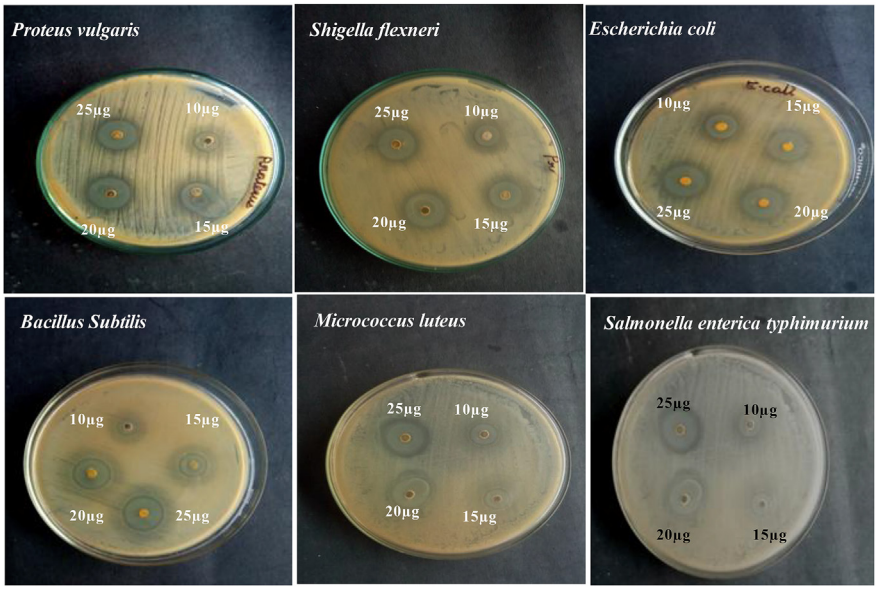

Fig. 6. Anti microbial activity of synthesized ZnO NPs.

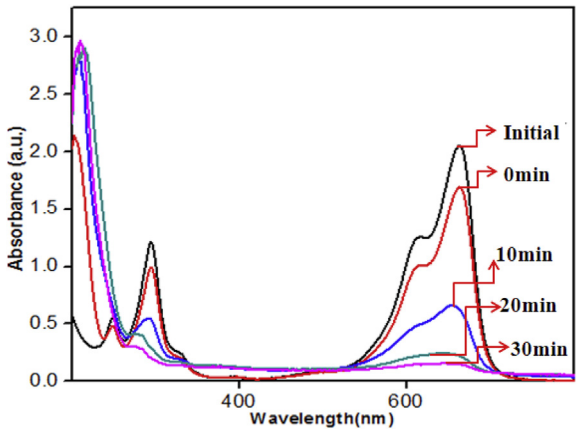

Fig. 7. Photocatalytic activity of synthesized ZnO NPs.

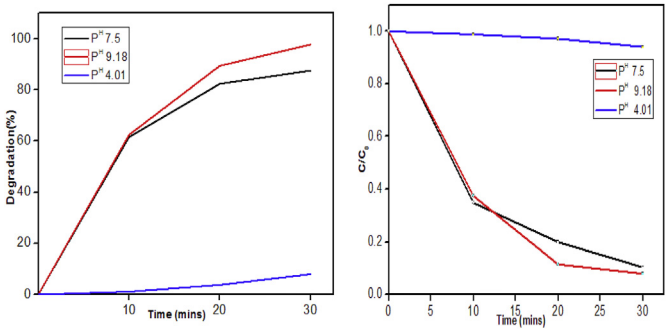

Fig. 8. Effects of pH on the photocatalytic activity of synthesized ZnO NPs.

and while increasing the pH to 7.8, the catalytic activity is also increased to 88.58% degradation while increasing the pH further towards basic (pH 9.8) the activity was good and reached up to 96% degradation (Fig. 8). The percentage of degradation by ZnO NPs synthesized was higher than that of some recent reports (Table 2).

It is known that the ZnO is a semiconducting material that has the conduction band (CB) electrons (e) and valence band (VB) holes (h+). These CB electrons and VB holes were generated by the ZnO when it was irradiated with light energy, which is higher than its band gap energy of Eg = 3.2 ev. These photo generated electrons are responsible for reduction of the dye and organics. They react with electron acceptors available in the reaction suspension like absorbed O_2 on the Zn (II) surface or O_2 dissolved in water and reducing them to super oxide radical anion O2-. The holes generated by photo catalyst ZnO will in turn oxidize the organic molecule MB or react with H_2O to produce OH radicals along with peroxide radicals that induced the photo degradation of MB. The OH radical produced during the reaction is a very potent oxidizer with standard redox potential of +2.8 V that can oxidize most of MB dye (Hoffman et al, 1995). Further higher basic pH is more favorable for the production OH free radical hence it will also support the catalytic activity.

4. Conclusions

In this research, we successfully synthesized ZnO NPs through a safe and ecofriendly green route using aqueous alcoholic extract of *Hydnocarpus alpina Wt*. Further extract of the plant subjected for the first time to GCMS phytochemical profiling and found 19 potential phytochemical in the extract. Results obtained from these green synthesized ZnO nano particles using HA extract demonstrated that ZNO NPs existed in a hexagonal (wurtzite) structure with a size of about 38 nm based on XRD and FE-SEM analyses. As expected, these prepared ZnO NPs showed excellent anti-microbial activities against all Gram

Table 2
Comparison of photocatalytic performance of HA mediated green synthesized ZnO NPs with recent reports.

	Catalyst synthesized	Plant utilized	Dye	Time of degradation (min)	% degraded	Refernces
1.	ZnO NPs	*Artocarpus gomezianus*	Methylene blue	120	90	Suresh et al. (2015)
2.	ZnO NPs	*Camellia sinensis*	Methylene blue	120	84	Nava et al. (2017)
3.	ZnO NPs	*Calotropis procera*	Methyl orange	100	81	Gawade et al. (2017)
4.	ZnO NPs	*Hydnocarpus alpina*	Methylene blue	30	96	Present work

(+)ve and Gram (−) microorganisms tested. These synthesized ZnO NPs showed more potential in inhibiting *Proteus vulgaris* and *Salmonella enterica typhimurium* compared to other microorganisms. Results of photocatalytic degradation of MB dye showed an irreversible color change from the original blue to colorless at basic pH with about 96% degradation which was higher than commercial bulk ZnO powder. Form the results it was concluded the that the plant HA has a higher potential to produce ZnO NPs in an eco friendly condition without any hazardous material, and the prepared ZnO NPs has also a wide scope of applications as a potent antimicrobial, antioxidant, and as a photo catalyst for degrading environmental pollutants such as dyes and chemicals.

Conflicts of interest

The authors declare that they have no conflicts of interest.

Acknowledgement

This work was financially supported by the Hanseo University Intramural Research Grant 2017. We would like to offer special thanks to Professor Sung Gil Lee, who, although no longer with us, for continues encouragement and support during the course of this study. We pray for Professor Sung Gil Lee welfare in the future life.

Appendix A. Supplementary data

Supplementary data to this article can be found online at https://doi.org/10.1016/j.bcab.2019.101129.

References

Alcorn, J.B., 1995. The scope and aims of ethnobotany in a developing world. In: Schultes, R.E., Reis, von S. (Eds.), Ethnobotany: Evolution of a Discipline. Chapman & Hall, London, pp. 23–39 1995.

Anandalakshmi, K., Venugobal, J., Ramasamy, V., 2016. Characterization of silver nanoparticles by green synthesis method using *Pedalium murex* leaf extract and their antibacterial activity. Appl. Nanosci. 6 (3), 399–408.

Anjugam, M., Vaseeharan, B., Iswarya, A., Divya, M., Prabhu, N.M., Sankaranarayanan, K., 2018a. Biological synthesis of silver nanoparticles using β-1, 3 glucan binding protein and their antibacterial, antibiofilm and cytotoxic potential. Microb. Pathog. 115, 31–40.

Anjugam, M., Vaseeharan, B., Iswarya, A., Gobi, N., Divya, M., Thangaraj, M.P., Elumalai, P., 2018b. Effect of β-1, 3 glucan binding protein based zinc oxide nanoparticles supplemented diet on immune response and disease resistance in Oreochromis mossambicus against Aeromonas hydrophila. Fish Shellfish Immunol. 76, 247–259.

Balamurugan, R., Ezhil Vendan, S., Aravinthan, A., Kim, J.-H., 2014. Isolation and structural characterization of 2R, 3R taxifolin 3-O-rhamnoside from ethyl acetate extract of *Hydnocarpus alpina* and its hypoglycemic effect by attenuating hepatic key enzymes of glucose metabolism in streptozotocin induced diabetic rats. Biochimie 111, 70–81.

Bisht, D., Owais, M., Venkatesan, K., 2006. Potential of plant-derived products in the treatment of mycobacterial infections. In: Ahmad, I., Aqil, F., Owais, M. (Eds.), Potential of Plant-Derived Products in the Treatment of Mycobacterial Infections. Wiley-VCH press, Weinheim, pp. 93–312.

Chang, H.-Y., Ho, Y.-L., Sheu, M.-J., Lin, Y.-H., Tseng, M.-C., Wu, S.-H., Huang, G.-J., Chang, Y.-S., 2007. Antioxidant and free radical scavenging activities of *Phellinus merrillii* extracts. Bot. Stud. 48, 407–417.

Chaudhuri, S.K., Malodia, L., 2017. Biosynthesis of zinc oxide nanoparticles using leaf extract of *Calotropis gigantea*: characterization and its evaluation on tree seedling growth in nursery stage. Appl. Nanosci. 7 (7), 501–512.

Chen, T., Wong, Y.S., Zheng, W., Bai, Y., Huang, L., 2008. Selenium nanoparticles fabricated in *Undaria pinnatifida* polysaccharide solutions induce mitochondria- mediated apoptosis in A375 human melanoma cells. Colloids Surfaces B Biointerfaces 67 (1), 26–31.

Davar, F., Majedi, A., Mirzaei, A., 2015. Green synthesis of ZnO nanoparticles and its application in the degradation of some dyes. J. Am. Ceram. Soc. 98, 1739–1746 2015.

Dhanasekaran, M., Karuppusamy, S., Annadurai, M., Rajasekaran, K.M., 2013. Evaluation of phytochemical constituents of Indian medicinal plant *Hydnocarpus alpina Wight*. Indian J. Pharm. Biol. Res. 1 (3), 23–28.

Dr.Duke's, 1992–2016. Phytochemical and Ethnobotanical Databases. U.S. Department of Agriculture, Agricultural Research Service. http://phytochem.nal.usda.gov, Accessed date: 20 November 2018.

Emami-Karvani, Z., Chehrazi, P., 2011. Antibacterial activity of ZnO nanoparticle on gram positive and gram-negative bacteria. Afr. J. Microbiol. Res. 5 (12), 1368–1373.

Ezhilvendan, S., Lingathurai, S., Gabriel Paulraj, M., Ignacimuthu, S., 2010. Ioefficacy of neem oil formulation with *Hydnocarpus Alpina* leaf extract against *Spodoptera litura*. Int . J. Current Res. 3, 78–82.

Fakim, G., 2006. Medicinal plants: traditions of yesterday and drugs of tomorrow. Mole. Aspects. Med. 2, 71–93.

Fawcett, D., Verduin, J.J., Shah, M., Sharma, S.B., Poinern, G.E.J., 2017. A review of current research into the Biogenic synthesis of metal and metal oxide nanoparticles via marine algae and seagrasses. J. Nanosci 1–15.

Gawade, V.V., Gavade, N.L., Shinde, H.M., Babar, S.B., Kadam, A.N., Garadkar, K.M., 2017. Green synthesis of ZnO nanoparticles by using Calotropis procera leaves for the photodegradation of methyl orange. Mater. Sci. Mater .Electron. 28 (18), 14033–14039.

Habib, M.A., Ismail, I.M.I., Mahmood, A.J., Ullah, M.R., 2012. Photocatalytic decolorization of brilliant golden yellow in TiO2 and ZnO suspensions. J. Saudi. Chemi.Soc 16 (4), 423–429.

Hoffmann, M.R., Martin, S.T., Choi, W., Bahnemannt, D.W., 1995. Environmental applications of semiconductor photocatalysis. Chem. Rev. 95 (1), 69–96.

Ingale, G., Chaudhari, A.N., 2013. Biogenic Synthesis of nanoparticles and potential applications: an eco friendly approach. J. Nanomed.Nanotechol. 4 (2), 165.

Iswarya, A., Vaseeharan, B., Anjugam, M., Ashokkumar, B., Govindarajan, M., Alharbi, N.S., Kadaikunnan, S., Khaled, J.M., Benelli, G., 2017. Multipurpose efficacy of ZnO nanoparticles coated by the crustacean immune molecule -1, 3-glucan binding protein: toxicity on HepG2 liver cancer cells and bacterial pathogens. Colloids Surfaces B Biointerfaces 158, 257–269.

Jiangnan, Y., Yingshu, F., Ximing, X., Shanshan, T.,.Hongfei, L., Yan, Y., 2013. Extract, preparation method and application of antitumor effective component from *Hydnocarpus hainanensis*. Faming Zhuanli Shenqing.Chinese patent : CN103027931A (2013).

Jose, G.S., Radhamany, P.M., 2012. Identification and determination of antioxidant constituents of bioluminescent mushroom. Asian. Pac. J. Trop. Biomed. S386–S391 2012.

Kondal Reddy, J., Sushmitha Rao, B., Shravani Reddy, T., Priyanka, B., 2013. Antidiabetic activity of ethanloic extract of *H. Wightiana blume* using STZ induced diabetes in Sd rats. J. Pharm. (Lahore) 23 (1), 29–40.

Mandal, T.K., Malhotra, S.P.K., Singha, R.K., 2018. Photocatalytic degradation of methylene blue in presence of ZnO nanopowders synthesized through a green synthesis method. Romanian J. Mater. 48 (1), 32–38.

Matinise, N., Fuku, X.G., Kaviyarasu, K., Mayedwa, N., Maaza, M., 2017. ZnO nanoparticles via Moringa oleifera green synthesis: physical properties and mechanism of formation. Appl. Surf. Sci. 406, 339–347.

Momeni, S.S., Nasrollahzadeh, M., Rustaiyan, A., 2016. Green synthesis of the Cu/ZnO nanoparticles mediated by *Euphorbia prolifera* leaf extract and investigation of their catalytic activity. J.Coll.Inter.Sci. 472, 173–179.

Nava, O.J., Luque, P.A., Comez-Gutierrez, C.M., Vilchis-Nestor, A.R., Castro-Beltrao, A., Mota- Gonzalez, M.L., Olivas, A., 2017. Influence of *Camellia sinensis* extract on Zinc Oxide nanoparticle green synthesis. J. Mol. Struct. 1134, 121–125.

Parthasarathy, N., 1999. Tree diversity and distribution in undisturbed and human- impacted sites of tropical wet evergreen forest in southern Western Ghat. Biodiver.Conserv. 8 (10), 1365–1381.

Ramesh, M., Anbuvannan, M., Viruthagiri, G., 2015. Green synthesis of ZnO nanoparticles using *Solanum nigrum* leaf extract and their antibacterial activity. Spectrochim.Acta. A. Mol. Biomol. Spectrosc. 136, 864–870.

Reddy, N.J., Nagoor Vali, D., Rani, M., Rani, S.S., 2014. Evaluation of antioxidant, antibacterial and cytotoxic effects of green synthesized silver nanoparticles by *Piper longum* fruit. Mater. Sci. Eng. C 34, 115–122 2014.

Sahoo, M.R., Dhanabal, S.P., Jadhav, A.N., Reddy, V., Muguli, G., Babu, U.V., Rangesh, 2014. P.,*Hydnocarpus*: anethnopharmacological, phytochemical and pharmacological review. J. Ethnopharmacol. 154, 17–25 2014.

Saravanakumar, A., Ganesh, M., Jayaprakash, J., Jang, H.T., 2015. Biosynthesis of silver nanoparticles using *Cassia tora* leaf extract and its antioxidant and antibacterial activities. J. Ind. Eng. Chem. 28, 277–281.

Saravanakumar, A., Peng, M.M., Ganesh, M., Jayaprakash, J., Mohankumar, M., Jang, H.T., 2017. Low- cost and eco-friendly green synthesis of silver nanoparticles using *Prunus japonica* (Rosaceae)leaf extract and their antibacterial,antioxidant properties. Artif. Cells. Nanomed. Biotechnol. 45, 1165–1171 2017.

Semwal, D.K., Bamola, A., Rawat, U., 2007. Chemical constituents of some antidiabetic plants. Univ. J. Phytochem. Ayur. Heights 2, 40–48.

Sharma, D., Rajput, J., Kaith, B.S., Kaur, M., Sharma, S., 2010. Synthesis of ZnO nanoparticles and study of their antibacterial and antifungal properties. Thin Solid Films 519 (3), 1224–1229.

Shriniwas, P.P., Subhash, T.K., 2017. Antioxidant, antibacterial and cytotoxic potential of silver nanoparticles synthesized using terpenes rich extract of *Lantana camara* L. leaves. Biochem. Biophys. Rep. 10, 76–81.

Song, H.Y., Ko, K.K., Oh, I.H., Lee, B.T., 2006. Fabrication of silver nanoparticles, and their antimicrobial mechanisms. Eur. Cells Mater. 11 (Suppl. 1), 58.

Sujitha, M.V., Kannan, S., 2013. Green synthesis of gold nanoparticles using Citrus fruits (*Citrus limon, Citrus reticulata* and *Citrus sinensis*) aqueous extract and its characterization. Spectrochim. Acta. Part. A Mole .Biomol. Spectrosc 102, 15–23.

Suresh, D., Shobharani, R.M., Nethravathi, P.C., Pavan Kumar, M.A., Nagabhushana, H., Sharma, S.C., 2015. Artocarpus gomezianus aided green synthesis of ZnO nanoparticles: luminescence, photocatalytic and antioxidant properties.Spectrochim. Acta Mol.Biomol. Spectrosc. 141, 128–134.

Thaya, R., Malaikozhundan, B., Vijayakumar, S., Sivakamavalli, J., Jeyasekar, R., Shanthi, S., Vaseeharan, B., Ramasamy, P., Sonawane, A., 2016. Chitosan coated Ag/ZnO nanocomposite and their antibiofilm, antifungal and cytotoxic effects on murine macrophages. Microb. Pathog. 100, 124–132.

Xiong, G., Pal, U., Serrano, J.G., Ucer, K.B., Williams, R.T., 2006. Photoluminescence and FTIR study of ZnO nanoparticles: the impurity and defect perspective. Phys. Status Solidi C 3 (10), 577–3581.